



## Original article

# Novel *N*-(3-carboxyl-9-benzyl- $\beta$ -carboline-1-yl)ethylamino acids: Synthesis, anti-tumor evaluation, intercalating determination, 3D QSAR analysis and docking investigation

Jianhui Wu<sup>a</sup>, Ming Zhao<sup>a,\*\*</sup>, Keduo Qian<sup>b</sup>, Kuo-Hsiung Lee<sup>b,\*\*\*</sup>,  
Susan Morris-Natschke<sup>b</sup>, Shiqi Peng<sup>a,\*</sup>

<sup>a</sup> College of Pharmaceutical Sciences, Capital Medical University, Beijing 100069, PR China

<sup>b</sup> Natural Products Research Laboratories, School of Pharmacy, University of North Carolina, Chapel Hill, NC 27599-7360, USA

## ARTICLE INFO

## Article history:

Received 4 December 2008

Received in revised form

1 May 2009

Accepted 7 May 2009

Available online 21 May 2009

## Keywords:

*N*-(3-Carboxyl-9-benzyl- $\beta$ -carboline-1-

yl)ethylamino acid

Anti-tumor activity

Intercalation

3D QSAR

Docking

## ABSTRACT

Sixteen novel *N*-(3-carboxyl-9-benzyl- $\beta$ -carboline-1-yl)ethylamino acids (**6a–p**) were synthesized as intercalating lead compounds. In the *in vitro* cytotoxic assay their IC<sub>50</sub> values against five human carcinoma cell lines ranged from 10.95  $\mu$ M to about 400  $\mu$ M. On S180 mouse model eight of them exhibited anti-tumor action, four of them showed the same anti-tumor potency as that of cytarabine. The preliminary toxicity evaluation revealed that the LD<sub>50</sub> values of **6a–p** should be more than 500 mg/kg. With CT DNA as model system an intercalating mechanism was explored. Using 3D QSAR analysis the relationship of the *in vivo* anti-tumor activity and the structure was quantitatively described. By docking **6a–p** onto d(CGATCG)<sub>2</sub> oligonucleotides the intercalation was demonstrated.

© 2009 Elsevier Masson SAS. All rights reserved.

## 1. Introduction

In medicinal chemistry, discovering new compounds with potent anticancer activity is one important goal. Among current anticancer chemotherapeutic agents DNA-recognizing molecules, including groove binders, alkylating compounds and intercalating agents, are particularly interesting. DNA intercalating agents are important in clinical oncology, and a few representative compounds (anthracyclines, acridines, and anthraquinones) are routinely used [1]. Structurally, DNA intercalating agents have a planar polycyclic aromatic pharmacophore capable of stacking between DNA pairs at the intercalation sites [2,3]. Intercalation results in conformational changes of the double helix, and then alters the processes of DNA replication, transcription and repair [4]. Thus the discovery of new DNA intercalating agents is considered as a promising approach toward anticancer drugs [5,6].

The synthesis and anticancer activities of a numerous compounds that intercalate into DNA have been reported recently [7–13]. Some  $\beta$ -carboline alkaloids such as harmine and its derivatives, are highly cytotoxic against human tumor cell lines [14–19]. In studies with  $\beta$ -carboline, DNA intercalation and cytotoxicity showed a correlation [20–23]. Thus,  $\beta$ -carboline act through intercalation to inhibit DNA topoisomerases I and II and cause DNA damage. As part of our ongoing efforts, we recently explored a series of  $\beta$ -carboline-3-carboxylamino acid benzyl ester conjugates as potent anticancer derivatives of natural products. We demonstrated that the *in vitro* cytotoxicity of the conjugates depended on all of their building blocks including  $\beta$ -carboline-3-carboxylic acid, amino acid and benzyl moieties [24]. On the other hand, the amino acid moieties of the conjugates are attractive because they not only possess structurally diverse side chains, but also are capable of improving pharmacokinetics of the conjugates. With this in mind, sixteen novel *N*-(3-carboxyl-9-benzyl- $\beta$ -carboline-1-yl)ethylamino acids **6a–p** were prepared in the present paper. These compounds were examined for their ability to inhibit the proliferation of human carcinoma cell lung carcinoma (H1299), liver carcinoma (HepG<sub>2</sub>), cervical carcinoma (Hela), immature granulocyte leukemia (HL-60) and human sarcoma (MES-SA) cells *in vitro*. Their *in vivo* anti-tumor

\* Corresponding author. Tel./fax: +86 10 8391 1528.

\*\* Corresponding author. Tel./fax: +86 10 8280 2482.

\*\*\* Corresponding author. Tel.: +1 919 962 0066; fax: +1 919 966 3893.

E-mail addresses: [khlee@unc.edu](mailto:khlee@unc.edu) (K.-H. Lee), [sqpeng@bjmu.edu.cn](mailto:sqpeng@bjmu.edu.cn) (S. Peng).

activities were assayed by using an S180 tumor-bearing mouse model (S180 mice). In order to examine their intercalating mechanism, **6b** was selected as a representative compound and CT DNA was selected as a DNA model to construct a simulation system for spectral analysis of UV, CD and fluorescence. To get insight into the correlation of the in vivo anti-tumor activity with the structure a corresponding 3D QSAR and docking were performed [25–29].

## 2. Results and discussion

### 2.1. Synthesis of *N*-(3-carboxyl-9-benzyl- $\beta$ -carboline-1-yl)ethylamino acids **6a–p**

Compounds **6a–p** were synthesized according to the seven-step route depicted in Scheme 1. Using a commonly used procedure, L-Trp was converted first to L-Trp-OMe (92% yield), and then to tetrahydro- $\beta$ -carboline-3-carboxylic acid methyl ester in 89% overall yield as a (1*S*, 3*S*) and (1*R*, 3*S*) diastereoisomeric mixture which could be resolved for analytical purposes by chromatography over silica gel. In the presence of KMnO<sub>4</sub>, the piperidine ring of **1** was aromatized to form  $\beta$ -carboline-3-carboxylic acid methyl ester (**2**) in 80% yield. Benzoylation at position-9 of **2** provided 9-benzyl- $\beta$ -carboline-3-carboxylic acid methyl ester (**3**, 61% yield). In the presence of HCl, HOAc and water **3** was underwent a hydrolysis and the acetal at position-1 was converted to an aldehyde, giving 2-(3-methoxycarbonyl-9-benzyl- $\beta$ -carboline-1-yl)acetaldehyde (**4**) in 61% yield. Coupling **4** with amino acid methyl esters followed by reduction of the coupling products provided 9-benzyl-1-carbonylmethyl- $\beta$ -carboline-3-carboxylamino acid methyl esters (**5a–o**), in yields ranging from 35% to 88%. However, coupling of **4** with glutamic dimethyl ester and consequent reduction failed to provide the desired 9-benzyl-1-carbonylmethyl- $\beta$ -carboline-3-carboxylglutamic acid trimethyl ester (**5p'**). Instead, only *N*-(3-carboxyl-9-benzyl- $\beta$ -carboline-1-yl)ethyl-5-oxotetrahydropyrole-2-carboxylic acid, the product of coupling and side chain cyclization (**5p**), was obtained in 67% yield. The saponification of **5a–p** provided 9-benzyl-1-carbonylmethyl- $\beta$ -carboline-3-carboxylamino acids (**6a–p**), in yields ranging from 52% to 72%. The mild conditions and

moderate yields of the individual reactions indicate that the present synthetic route should be suitable for preparing these novel compounds and their analogs.

### 2.2. Anti-tumor activities of **6a–p**

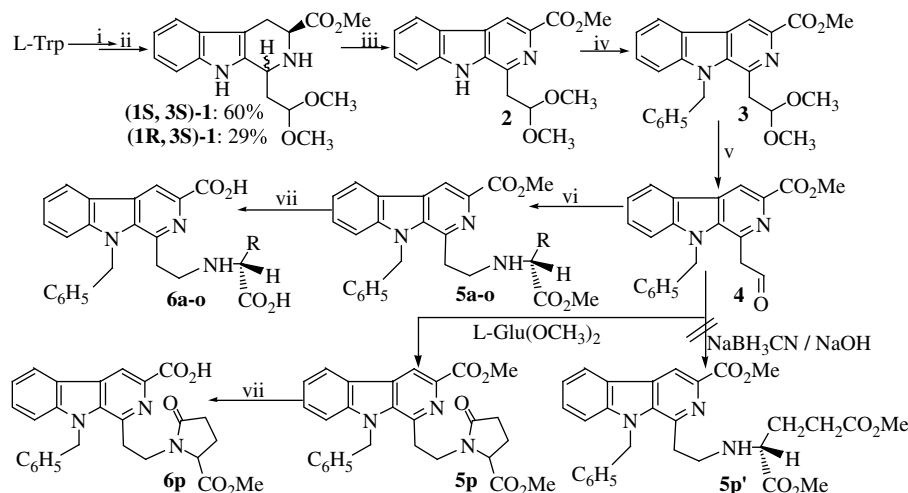
In the evaluation of the in vitro anti-tumor activity, anti-proliferation assays with serial concentrations of **6a–p** in NS against H1299, HepG<sub>2</sub>, Hela, HL-60 and MES-SA cells were performed. In the evaluation of the in vivo anti-tumor activities of **6a–p**, their effects on the tumor weights of S180 mice were determined. In the examination of the dose-dependent action of **6a–p** the most potent compound (**6b**) was selected as the representative compound to observe the dose-dependent action.

#### 2.2.1. IC<sub>50</sub> of **6a–p** against the proliferation of five human carcinoma cells

In the anti-proliferation assays, H1299, HepG<sub>2</sub>, Hela, HL-60 and MES-SA cells were exposed to serial concentrations (0.1–400  $\mu$ M) of **6a–p**, and standard MTT assays were performed. The IC<sub>50</sub> values of **6a–p** against the five cell lines are summarized in Table 1. The data indicate that **6a–p** selectively inhibit these five carcinoma types. The highest potencies were found against MES-SA cells, and with IC<sub>50</sub> values ranging from 11.0 to 14.5  $\mu$ M, **6a,e,l,o** were more potent than the remaining compounds. Compounds **6a,b,h,i,k,n** exhibited the lowest IC<sub>50</sub> values (ranging from 23.5 to 33.2  $\mu$ M) against HL-60 cells. Compound **6o** was the most potent (IC<sub>50</sub> = 20.0  $\mu$ M) against H1299 cells, and **6g** was the most potent (IC<sub>50</sub> = 26.5  $\mu$ M) against Hela cells. However, HepG<sub>2</sub> cells were less sensitive than the other four cell lines to these compounds; no IC<sub>50</sub> values were less than 70  $\mu$ M against this cell line.

#### 2.2.2. In vivo activities of **6a–p** on S180 mouse model

In the in vivo anti-tumor assays, the tumor weights of S180 mice receiving **6a–p** were recorded. As shown in Table 2, when the mice were given a daily i.p injection of 89  $\mu$ mol/kg of **6a–p** in 0.2 ml of NS for seven consecutive days, their tumor weights ranged from 2.12 g to 0.74 g (NS receiving mice, 1.65 g). Eight compounds significantly



**Scheme 1.** Synthesis of *N*-(3-carboxyl-9-benzyl- $\beta$ -carboline-1-yl)ethylamino acids **6a–o**. Reaction conditions: (i) SOCl<sub>2</sub>, MeOH; (ii) HCl, 1,1,3,3-tetramethoxypropane, MeOH; (iii) KMnO<sub>4</sub>, DMF; (iv) NaH, BrCH<sub>2</sub>C<sub>6</sub>H<sub>5</sub>, DMF/THF; (v) HCl, HOAc, H<sub>2</sub>O; (vi) NaOH, NaBH<sub>3</sub>CN and L-Phe-OMe or L-Ala-OMe or Gly-OMe or L-Arg or L-Asp-OMe or L-Leu-OMe or L-Met-OMe or L-Ser-OMe or L-Tyr-OMe or L-Thr-OMe or L-Ile-OMe or L-Trp-OMe or L-Val-OMe or L-Pro-OMe or L-His-OMe; (vii) NaOH/MeOH. **5a** and **6a** R = CH<sub>2</sub>C<sub>6</sub>H<sub>5</sub>, **5b** and **6b** R = CH<sub>3</sub>, **5c** and **6c** R = H, **5d** and **6d** R = CH<sub>2</sub>(CH<sub>2</sub>)<sub>2</sub>NH(NH<sub>2</sub>)=NH, **5e** R = CH<sub>2</sub>CO<sub>2</sub>CH<sub>3</sub>, **5f** R = CH<sub>2</sub>CO<sub>2</sub>H, **5g** and **6g** R = CH<sub>2</sub>CH(CH<sub>3</sub>)<sub>2</sub>, **5h** and **6h** R = CH<sub>2</sub>CH<sub>2</sub>SCH<sub>3</sub>, **5i** and **6i** R = CH<sub>2</sub>C<sub>6</sub>H<sub>4</sub>-OH, **5j** and **6j** R = CH(OH)CH<sub>3</sub>, **5k** and **6k** R = CH(CH<sub>3</sub>)CH<sub>2</sub>CH<sub>3</sub>, **5l** and **6l** R = indole-3-ylmethylene, **5m** and **6m** R = CH(CH<sub>3</sub>)<sub>2</sub>, **5n** and **6n** R = NH=NCH<sub>2</sub>CH<sub>2</sub>, **5o** and **6o** R = imidazole-3-ylmethylene.

**Table 1**  
IC<sub>50</sub> of **6a–p** against HL-60, Hela, H1299, HepG<sub>2</sub> and MES-SA cell lines.

Compd <sup>a</sup>	HL-60	Hela	H1299	HepG <sub>2</sub>	MES-SA
<b>6a</b>	31.8 ± 10.6	51.7 ± 8.8	59.3 ± 7.5	114.0 ± 7.0	11.0 ± 3.7
<b>6b</b>	28.1 ± 7.5	122.0 ± 11.0	81.8 ± 8.3	242.0 ± 6.9	120.0 ± 6.5
<b>6c</b>	>400.0	>400.0	75.6 ± 9.4	>400.0	178.0 ± 3.0
<b>6d</b>	40.9 ± 6.7	259.0 ± 8.4	86.4 ± 6.2	161.0 ± 3.0	68.2 ± 8.5
<b>6e</b>	43.2 ± 8.4	99.3 ± 4.0	69.0 ± 10.7	114.0 ± 2.4	13.0 ± 0.8
<b>6f</b>	45.2 ± 3.6	189.0 ± 13.5	69.9 ± 7.5	176.0 ± 23.1	71.2 ± 3.8
<b>6g</b>	182.0 ± 6.0	26.5 ± 1.3	100.0 ± 10.0	108.0 ± 8.0	86.4 ± 15.9
<b>6h</b>	23.5 ± 7.6	210.0 ± 13.0	83.8 ± 8.7	174.0 ± 12.0	136.0 ± 3.0
<b>6i</b>	24.0 ± 1.4	209.0 ± 17.0	72.5 ± 4.4	127.0 ± 4.0	59.3 ± 4.9
<b>6j</b>	50.4 ± 11.2	221.0 ± 24.0	86.4 ± 0.6	>400.0	218.0 ± 11.0
<b>6k</b>	33.2 ± 2.6	200.0 ± 19.0	69.0 ± 9.0	254.0 ± 14.0	181.0 ± 15.0
<b>6l</b>	102.0 ± 4.0	393.0 ± 20.0	57.3 ± 3.3	107.0 ± 5.0	11.7 ± 4.0
<b>6m</b>	>400.0	290.0 ± 9.0	199.0 ± 7.0	>400.0	175.0 ± 2.0
<b>6n</b>	28.4 ± 8.2	161.0 ± 8.0	75.5 ± 1.7	107.0 ± 1.2	55.2 ± 2.3
<b>6o</b>	160.0 ± 63.0	136.0 ± 12.0	20.0 ± 1.3	70.7 ± 2.0	14.5 ± 1.0
<b>6p</b>	112.0 ± 19.0	>400.0	97.6 ± 12.6	>400.0	45.9 ± 12.0

<sup>a</sup> IC<sub>50</sub> value is expressed by  $\bar{x} \pm SD$   $\mu$ M and  $n = 6$ .

decreased the tumor weights of the S180 mice, compounds **6b,i,l,m** (tumor weights ranging from 0.74 g to 0.85 g) were essentially equipotent to the positive control cytarabine (tumor weight 0.74 g). Compounds **6d,e,h,p** decreased the tumor load (tumor weights ranging from 1.08 g to 0.94 g), but were less potent than the positive control.

The anti-tumor action likely correlates with the identity of the 1-substituent (R group). The active compounds contained either a small aliphatic group (methyl and isopropyl) or an acidic group (carboxymethyl, 5-oxotetrahydropyrole-2-carboxylic acid and phenol) or a basic group (guanidopropyl and indole).

### 2.2.3. Dose dependent in vivo anti-tumor activities of **6b**

The most potent compound (**6b**) was selected as the model compound to examine the dose-dependent action of **6a–p**. At doses of 0.0089, 0.89 and 89.0  $\mu$ mol/kg, it showed dose-dependent inhibition with percentages of 1.5%, 25.6%, and 55.2%, respectively (Table 3). Therefore, **6b** possesses significant anti-tumor potency at doses above 89  $\mu$ mol/kg.

### 2.3. Toxicity of **6a–e,i–k** on mice

To evaluate the preliminary toxicity of **6a–p** during the administration the spleen index of the mice was measured and used to reflect the immunologic function, the body weights of the mice were measured and used to reflect the health, and the acute toxicity of some representatives including the most potent and least potent compounds was measured and used to estimate LD<sub>50</sub> values.

**Table 2**  
Effects of **6a–p** on tumor weights of S180 mice.

Compd <sup>a</sup>	% Inhibition	Tumor weight	Compd	% Inhibition	Tumor weight
<b>6a</b>	5.2 ± 1.4	1.56 ± 0.42	<b>6i</b>	48.6 ± 12.3	0.85 ± 0.21 <sup>b</sup>
<b>6b</b>	55.2 ± 6.7	0.74 ± 0.09 <sup>b</sup>	<b>6j</b>	−29.1 ± 5.4	2.12 ± 0.41
<b>6c</b>	11.0 ± 2.4	1.47 ± 0.32	<b>6k</b>	1.6 ± 0.2	1.62 ± 0.22
<b>6d</b>	37.7 ± 8.1	1.03 ± 0.22 <sup>c</sup>	<b>6l</b>	47.2 ± 13.3	0.85 ± 0.23 <sup>b</sup>
<b>6e</b>	34.7 ± 4.8	1.08 ± 0.15 <sup>c</sup>	<b>6m</b>	53.8 ± 19.4	0.76 ± 0.28 <sup>b</sup>
<b>6f</b>	8.7 ± 1.9	1.51 ± 0.32	<b>6n</b>	7.2 ± 1.9	1.53 ± 0.43
<b>6g</b>	1.5 ± 0.3	1.63 ± 0.28	<b>6o</b>	9.7 ± 2.1	1.49 ± 0.32
<b>6h</b>	35.3 ± 6.9	1.07 ± 0.21 <sup>c</sup>	<b>6p</b>	43.0 ± 7.4	0.94 ± 0.16 <sup>c</sup>
Ara-C	54.8 ± 14.5	0.74 ± 0.20	NS		1.65 ± 0.49

<sup>a</sup> Dose of Ara-C (cytarabine) and **6a–p**: 89  $\mu$ mol/kg, NS = vehicle,  $n = 12$ , tumor weight is expressed by  $\bar{x} \pm SD$  g.

<sup>b</sup> Compared to NS  $p < 0.01$ , to Ara-C  $p > 0.05$ .

<sup>c</sup> Compared to NS  $p < 0.01$ , to Ara-C  $p < 0.05$ .

**Table 3**  
Anti-tumor activity of **6b** at different doses against S180 mice.

Compd <sup>a</sup>	Dose ( $\mu$ mol/kg)	Tumor weight (g)	% Inhibition
<b>6b</b>	89.00	0.74 ± 0.09 <sup>b</sup>	55.2 ± 6.7 <sup>b</sup>
<b>6b</b>	0.89	1.22 ± 0.27 <sup>c</sup>	25.6 ± 5.8 <sup>c</sup>
<b>6b</b>	0.0089	1.64 ± 0.38	1.5 ± 0.3
Ara-C	89.00	0.74 ± 0.20	54.8 ± 14.5
NS		1.65 ± 0.49	

<sup>a</sup> Ara-C = positive control, NS = vehicle,  $n = 12$ .

<sup>b</sup> Compared to NS and 0.89  $\mu$ mol/kg of **6b**  $p < 0.01$ .

<sup>c</sup> Compared to NS and 0.0089  $\mu$ mol/kg of **6b**  $p < 0.05$ .

### 2.3.1. Spleen index and body weight of S180 mice receiving **6a–p**

Immunologic function is important to chemotherapy and spleen index is an important parameter of the immunologic function. Therefore, the spleen indexes of **6a–p** receiving S180 mice were measured. The data are listed in Table 4. The comparison of the spleen index of the S180 mice receiving NS and synthetic compounds **6a–p** demonstrates that most of the compounds did not change the immunologic function of the S180 mice. Exceptions were **6a,i**, which enhanced immunologic function.

During chemotherapy, an increase body weight is an important parameter of health. Thus, the body weights of the mice receiving **6a–p** were measured. The data are listed in Table 4 as increase body weight from start of treatment. Compounds **6b–e,h–p** showed weight gain similar to that of the vehicle-treat group. Only three compounds (**6a,f,g**) showed significantly lower increases in body weight.

### 2.3.2. Acute toxicity of mice receiving **6a–e,i–k**

Most of the reported 9-substituted- $\beta$ -carboline were known as a class of strong neurotoxic and low survival indole alkaloids, and the discovery of comparatively non-toxic and highly survival  $\beta$ -carboline as intercalators has been particularly interesting [29]. To know the toxic level of **6a–p** the representative compounds **6a–e,i–k** were examined for the LD<sub>50</sub> and neurotoxicity in mice model. The results indicate that even the dose of **6a–e,i–k** was up to 500 mg/kg the mice neither exhibited neurotoxic behavior, such as tremor, twitch, jumping, tetanus, and supination, nor occurred death. Necropsy findings in **6a–e,i–k** receiving mice on the 7th day revealed that the administration led no apparent changes in any organs. These suggest that **6a–e,i–k** are comparatively non-toxic, and their LD<sub>50</sub> values should be more than 500 mg/kg.

### 2.4. Intercalation of **6a–d** toward CT DNA

Different DNA spectra have been widely used to explore its intercalation with small molecules. In order to confirm the

**Table 4**  
Effect of **6a–p** on the spleen index and body weight increase of S180 mice.

Compd <sup>a</sup>	Spleen index	Increased BW	Compd <sup>a</sup>	Spleen index	Increased BW
<b>6a</b>	14.41 ± 1.23 <sup>b</sup>	9.74 ± 2.26 <sup>b</sup>	<b>6i</b>	13.62 ± 1.51 <sup>b</sup>	13.62 ± 1.51
<b>6b</b>	13.32 ± 1.34	12.92 ± 1.39	<b>6j</b>	11.37 ± 2.12	11.37 ± 2.12
<b>6c</b>	13.13 ± 2.18	11.34 ± 2.10	<b>6k</b>	13.56 ± 1.76	13.56 ± 1.76
<b>6d</b>	12.65 ± 1.89	11.19 ± 2.78	<b>6l</b>	11.67 ± 1.23	11.67 ± 1.23
<b>6e</b>	12.99 ± 1.29	10.11 ± 3.74	<b>6m</b>	10.23 ± 1.52	10.23 ± 1.52
<b>6f</b>	10.87 ± 2.10	9.04 ± 3.10 <sup>b</sup>	<b>6n</b>	12.07 ± 2.83	12.07 ± 2.83
<b>6g</b>	11.80 ± 3.85	9.12 ± 3.29 <sup>b</sup>	<b>6o</b>	11.87 ± 2.07	11.87 ± 2.07
<b>6h</b>	10.49 ± 0.89	11.46 ± 2.81	<b>6p</b>	12.24 ± 1.10	12.24 ± 1.10
Ara-C	10.17 ± 3.32	9.65 ± 2.50 <sup>b</sup>	NS	11.84 ± 2.34	12.32 ± 2.94

<sup>a</sup> Dose of Ara-C (cytarabine) and **6a–p**: 89  $\mu$ mol/kg, NS = vehicle,  $n = 12$ , spleen index is expressed by  $\bar{x} \pm SD$  mg/kg body weight, increased BW = increased body weight is expressed by  $\bar{x} \pm SD$  g.

<sup>b</sup> Compared to NS  $p < 0.05$ .

intercalation of **6a–p**, calf thymus DNA (CT DNA) was selected as the model DNA, **6b** was selected as model compound of **6a–p**, and a combination of CT DNA and **6b** was selected as model system for simulating the interactions of **6a–p** toward DNA. UV, CD and fluorescence spectra were measured with this simulation system. The results provided important spectral evidence for intercalation of **6b** with CT DNA, and also prove that this simulation system should be generally useful to define intercalation of  $\beta$ -carboline with DNA.

#### 2.4.1. UV spectra defined intercalation **6b** with CT DNA

The UV spectra of a solution of CT DNA alone in PBS buffer (pH 7.4, final concentration, 240  $\mu$ M) and a solution of CT DNA (pH 7.4, final concentration, 240  $\mu$ M) plus the representative compound **6b** (final concentration, 20  $\mu$ M) in PBS buffer were determined on a Shimadzu 2550 spectrophotometer from 220 to 350 nm. Fig. 1 shows the two spectra obtained. Compound **6b** induced a hypochromic effect (47.0%) and bathochromic shift (3.2 nm) compared with the UV spectrum of CT DNA alone. Hypochromic effects and bathochromic shifts are considered to be evidence of intercalation of DNA with small molecules [30]. Thus the UV changes seen in UV experiment are direct evidence for intercalation of **6b** with CT DNA.

#### 2.4.2. CD spectra defined intercalation of **6b** with CT DNA

The circular dichroic (CD) spectrum of CT DNA is characterized by positive and negative bands. The former band is due to base stacking and the latter band is due to right-handed helicity. The two bands change in intensity as the result of intercalation interactions of CT DNA with small molecules [31,32]. In our CD experiments a solution of CT DNA alone in PBS buffer (pH 7.4, final concentration, 40  $\mu$ M) and a solution (pH 7.4) of CT DNA (final concentration, 40  $\mu$ M) plus the representative compound **6b** (final concentration, 100  $\mu$ M) in PBS buffer were incubated at 37  $^{\circ}$ C for 24 h, and then their CD spectra were obtained according to the standard procedure. The parameters of the CD spectra are given in Fig. 2. At 100  $\mu$ M, **6b** induced an intensity increase in the positive band (molecular ellipticities  $[\theta]$  for CT DNA alone = 18,909  $\text{deg cm}^2 \text{dmol}^{-1}$ ;  $[\theta]$  for DNA + 100  $\mu$ M **6b** = 26,523  $\text{deg cm}^2 \text{dmol}^{-1}$ ) and an intensity decrease in the negative band ( $[\theta]$  for CT DNA alone = -21,020  $\text{deg cm}^2 \text{dmol}^{-1}$ ;  $[\theta]$  for CT DNA + 100  $\mu$ M **6b** = -9685  $\text{deg cm}^2 \text{dmol}^{-1}$ ). These observations reflect intercalation of **6b** with CT DNA, characterized by decreasing both the base stacking and the right-handedness of CT DNA.

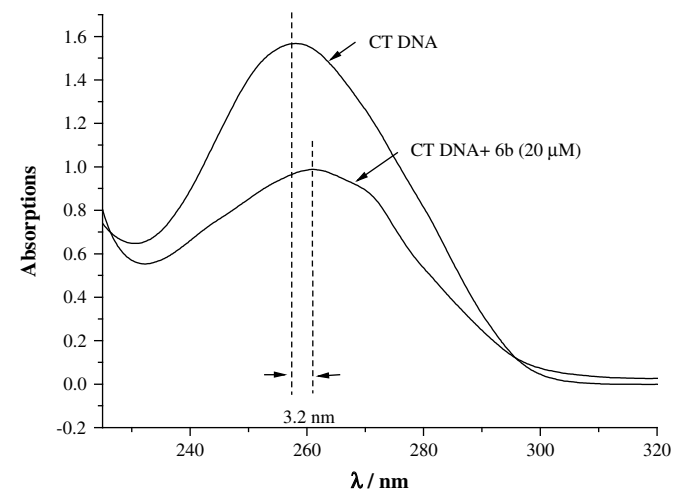


Fig. 1. UV spectra of CT DNA without and with **6b** in PBS buffer (pH = 7.4).

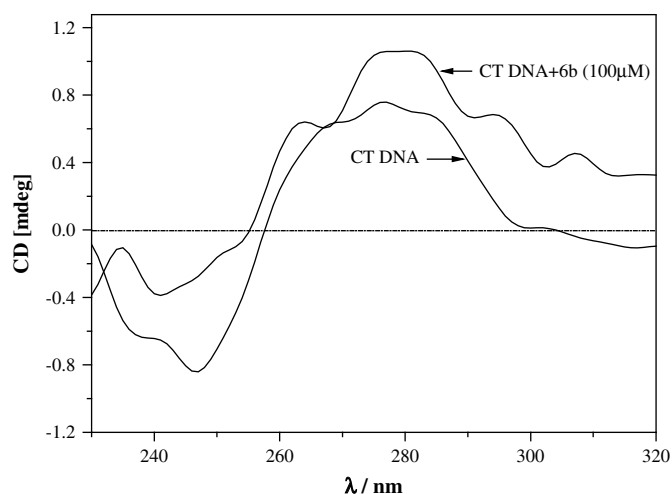


Fig. 2. CD spectra of CT DNA without and with **6b**.

#### 2.4.3. Fluorescence spectra defined intercalation of **6b** with CT DNA

To further confirm the intercalating mechanism of **6a–p**, the effect of CT DNA on the fluorescence intensity of **6b** was determined at 300 K by the use of fluorescence spectroscopy. In the determinations, a solution of **6b** in PBS buffer (0.5  $\mu$ M, pH = 7.4) was titrated with 10  $\mu$ l of solutions containing serial concentrations (0, 8, 16, 24, 32, 40, 48, 56, 64 and 72  $\mu$ M, pH = 7.4) of CT DNA in PBS buffer. The corresponding changes in the fluorescence intensity of **6b** were observed on a Shimadzu RF-5310PC spectrofluorometer at a fluorescence excitation wavelength of 245 nm. CT DNA caused a concentration-dependent decrease in the fluorescence intensities (fluorescence quenching) of **6b**. Fig. 3 illustrates the typical course of the fluorescence quenching, the fluorescence intensity of **6b** gradually decreased as the concentration of added CT DNA gradually increased. When the concentration of added CT DNA was increased to 72  $\mu$ M, the fluorescence intensity of **6b** was lowered to its minimum. At this point, the fluorescence intensity had decreased by 59.09%. Over the course of the fluorescence quenching, a slight bathochromic shift was also noticed as seen in Fig. 3. This bathochromic shift is considered to be associated with a decrease in the energy gap between the highest and lowest

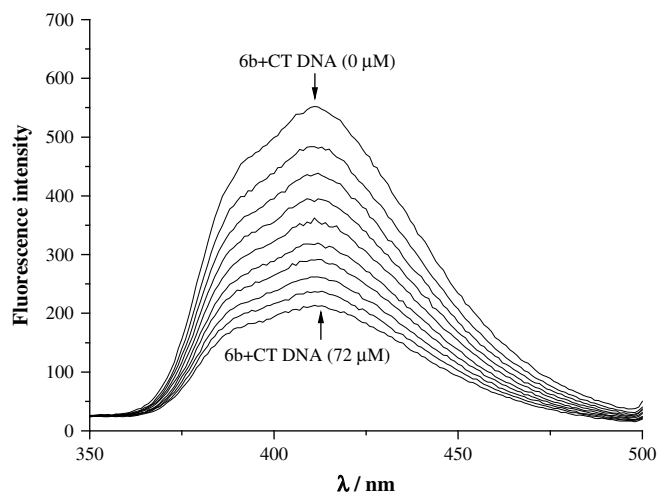


Fig. 3. Fluorescence spectra of **6b** (concentration 0.5  $\mu$ M, pH = 7.4,  $\lambda_{\text{max}} = 254$  nm) with serial concentrations (0, 8, 16, 24, 32, 40, 48, 56, 64, 72  $\mu$ M) of CT DNA in PBS buffer.

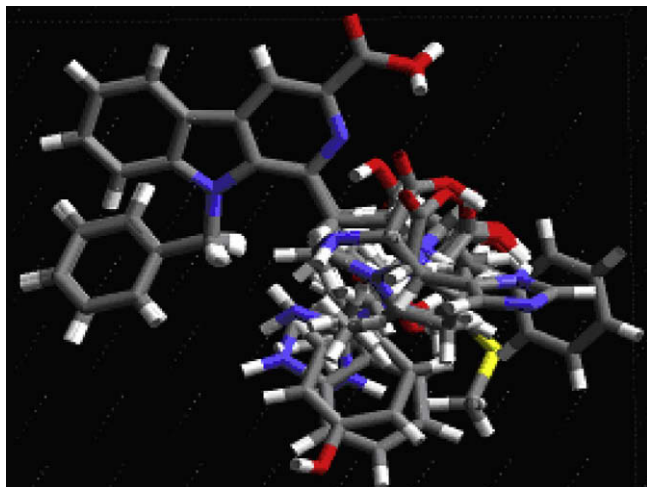


Fig. 4. Alignment stereoview of **6a-p** used for molecular field generation.

occupied molecular orbitals, and results from intercalation of **6b** with CT DNA [33].

### 2.5. 3D QSAR analysis of **6a-p**

To correlate the structure of **6a-p** with the tumor weights of the mice receiving them a 3D QSAR analysis was performed by use of Cerius<sup>2</sup> module and following standard procedure.

#### 2.5.1. Alignment of **6a-p**

To establish valid 3D QSAR models a proper alignment procedure of **6a-p** was performed using the target model align strategy in the align module within Cerius<sup>2</sup>. With an assumption that each structure of **6a-p** binds the same site of the receptor and exhibits activity, they were aligned in a pharmacological active orientation. To obtain a consistent alignment, the common 9-benzyl- $\beta$ -carboline-3-carboxylic acid moiety was selected as the template for superposing **6a-p**. The method used for performing the alignment was the maximum common subgraph (MCS) [34]. MCS looks at molecules as points and lines, and uses the techniques out of graph theory to identify the patterns. Then MCS finds the largest subset of atoms in

9-benzyl- $\beta$ -carboline-3-carboxylic acid that shared by **6a-p**. This subset was used for the alignment. A rigid fit of atom pairings was performed to superimpose each structure onto the target model 9-benzyl- $\beta$ -carboline-3-carboxylic acid. Stereoview of aligned **6a-p** is shown in Fig. 4. The alignment stereoview explores that to superimpose onto 9-benzyl- $\beta$ -carboline-3-carboxylic acid the 2-group, ethylamino acid, of each structure has to take individual conformation. This individual conformation of the 2-group will influence on the anti-tumor activity.

#### 2.5.2. QSAR module of Cerius<sup>2</sup> based MFA of **6a-p**

Molecular field analysis (MFA) was performed for **6a-p** using the QSAR module of Cerius<sup>2</sup> [35]. A five-step procedure consisted of generating conformers, energy minimization, matching atoms and aligning molecules, setting preferences, and regression analysis was automatically practiced in MFA. Molecular electrostatic and steric fields were created by use of proton and methyl groups as probes, respectively. These fields were sampled at each point of a regularly spaced grid of 1 Å. An energy cutoff of  $\pm 30.0$  kcal/mol was set for both electrostatic and steric fields. The total grid points generated were 672. Though the spatial and structural descriptors such as dipole moment, polarizability, radius of gyration, number of rotatable bonds, molecular volume, principal moment of inertia, AlogP98, number of hydrogen bond donors and acceptors, and molar refractivity were also considered, only the highest variance holder proton, methyl and hydroxyl descriptors were used. Regression analysis was carried out using the genetic partial least squares (G/PLS) method consisting of 50,000 generations with a population size of 100. The number of components was set to 5. Cross-validation was performed with the leave-one-out procedure. PLS analysis was scaled, with all variables normalized to a variance of 1.0.

The regions where variations in the steric or electrostatic features of **6a-p** in the training set lead to increase or decrease activities were specified. Proton descriptor with positive coefficient indicates a region favorable for electropositive group, while negative coefficient indicates electronegative group required at this position. Methyl descriptor with positive coefficient indicates a region favorable for large group, while negative coefficient indicates small group required at this position. Hydroxyl descriptor with positive coefficient indicates a region favorable for hydrogen bond forming group, while negative coefficient indicates hydrogen bond forming group not required at this position. The MFA model for the activity of **6a-p** in terms of the most relevant descriptors proton and methyl group is expressed by Equation (1).

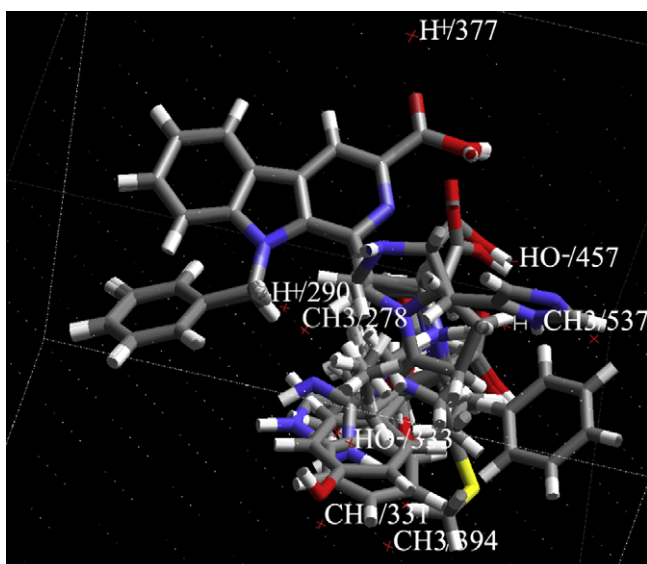


Fig. 5. Alignment stereoview of **6a-p** influencing on in vivo anti-tumor activity.

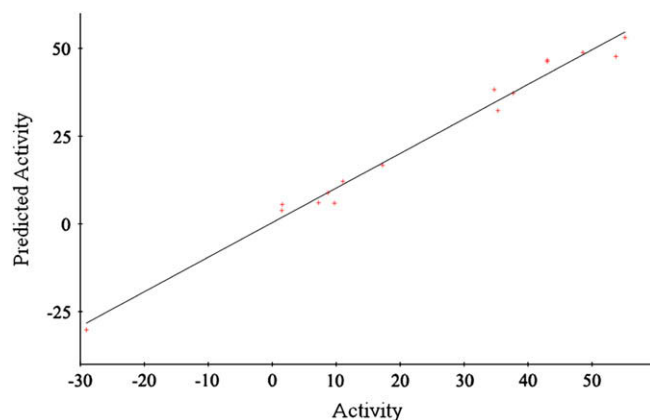
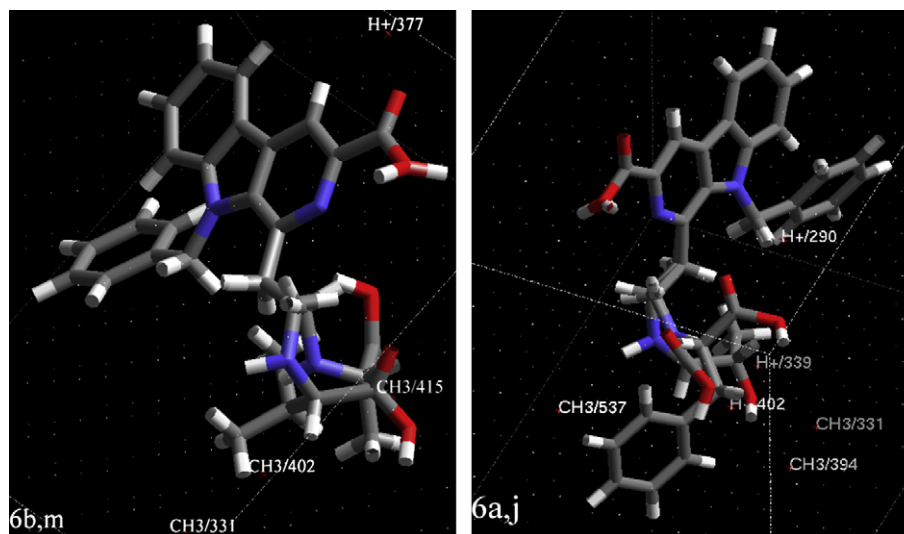


Fig. 6. Graph of tested inhibition against predicted inhibition of anti-tumor activities in vivo.



**Fig. 7.** Electrostatic environment of **6b** and **6m** with high in vivo anti-tumor activities, as well as **6a** and **6j** with low in vivo anti-tumor activities within the grid with 3D points of Equation (1).

$$\begin{aligned}
 \text{Inhibition} = & 65.9465 + 0.263568(\text{H}^+/389) \\
 & - 0.296122(\text{H}^+/377) - 0.616359(\text{H}^+/339) \\
 & - 0.670101(\text{H}^+/402) - 0.175716(\text{H}^+/290) \\
 & + 1.15455(\text{CH}_3/331) + 1.20715(\text{CH}_3/402) \\
 & - 1.51675(\text{CH}_3/415) - 0.691845(\text{CH}_3/394) \\
 & - 0.233533(\text{CH}_3/537) - 0.757249(\text{CH}_3/278) \\
 & - 1.15548(\text{OH}^-/474) - 0.813747(\text{OH}^-/487) \\
 & + 0.252125(\text{OH}^-/333)
 \end{aligned} \quad (1)$$

The correlation of the activities tested on the in vivo anti-tumor model and the activities calculated using Equation (1) is explained by Fig. 5 ( $r^2$ , 0.985). The data points ( $n$ ), correlation coefficient ( $r$ ) and square correlation coefficient ( $r^2$ ) of Equation (1) were 16, 0.992 and 0.985, respectively. The correlation of the anti-tumor activities tested on S180 mouse model and calculated from Equation (1) is explained by Fig. 6.

In Equation (1) one term of  $\text{H}^+/389$  with positive coefficient from proton descriptor, which means that at this position electron-releasing group will increase the in vivo anti-tumor activity, four terms of  $\text{H}^+/377$ ,  $\text{H}^+/339$ ,  $\text{H}^+/402$ ,  $\text{H}^+/290$  with negative coefficient from proton descriptor, which means that at these positions electron-releasing group will decrease the in vivo anti-tumor activity, two terms of  $\text{CH}_3/331$ ,  $\text{CH}_3/402$  with positive coefficient from

methyl descriptor, which means that at these positions large group will increase the in vivo anti-tumor activity, four terms of  $\text{CH}_3/415$ ,  $\text{CH}_3/394$ ,  $\text{CH}_3/537$ ,  $\text{CH}_3/278$  with negative coefficient from methyl descriptor, which means that at these positions large group will decrease the in vivo anti-tumor activity, one term of  $\text{OH}^-/333$  with positive coefficients from hydroxyl descriptor, which means that at this position electron-withdrawing group will increase the in vivo anti-tumor activity, and two terms of  $\text{OH}^-/474$ ,  $\text{OH}^-/487$  with negative coefficients from hydroxyl descriptor, which means that at these positions electron-releasing groups will increase the in vivo anti-tumor activity, are involved.

As examples Fig. 7 gives the electrostatic environments of representatives **6b** and **6m** with high in vivo anti-tumor activities, as well as **6a** and **6j** with low in vivo anti-tumor activities within the grid with 3D points of Equation (1). Besides the same electrostatic and environments as 9-benzyl- $\beta$ -carboline-3-carboxylic acid moiety **6b** has small group near  $\text{CH}_3/415$  and thus resulting in increasing the in vivo anti-tumor activity, and **6m** has large group near  $\text{CH}_3/402$ , thus also resulting in increasing the in vivo anti-tumor activity. Besides the same electrostatic and environments as 9-benzyl- $\beta$ -carboline-3-carboxylic acid moiety **6a** has large group near  $\text{CH}_3/394$ ,  $\text{CH}_3/537$  and thus resulting in decreasing the in vivo anti-tumor activity, and **6j** has both electron-releasing and electron-withdrawing groups near  $\text{H}^+/339$ , thus totally resulting in no change of the in vivo anti-tumor activity.

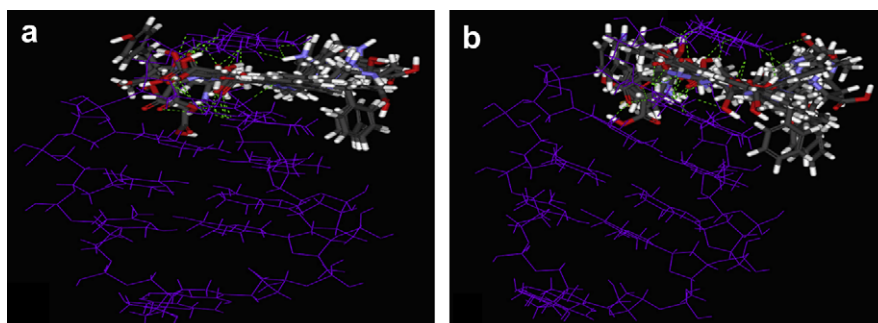


**Fig. 8.** (a) Stereoview of **6b,d,e,h,i,l,m,p** with in vivo anti-tumor activity intercalating toward  $d(\text{CGATCG})_2$ , and (b) stereoview of **6a,c,f,g,j,k,n,o** without in vivo anti-tumor activity intercalating toward  $d(\text{CGATCG})_2$ .

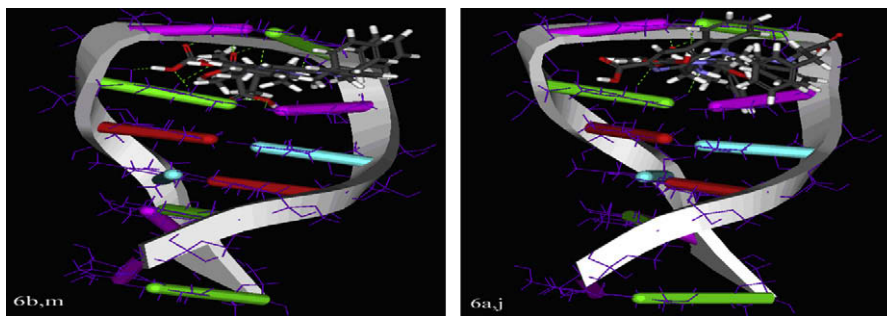


Fig. 9. The docking interactions of the most potent compounds **6b,m** and the least potent compounds **6a,j** with  $d(\text{CGATCG})_2$ .

## 2.6. Docking **6a–p** onto $d(\text{CGATCG})_2$ oligonucleotides

As one of the most important molecular-cellular targets of several anticancer drugs DNA can be conveniently intercalated by heterocycle having a planar structure [36]. To further explore the dependence of the anti-tumor activity on the structure the automated docking studies of **6a–p** were performed using the Ligand-Fit/LigandScore in Discovery Studio (DS) Modeling 2.1.  $d(\text{CGATCG})_2$  oligonucleotide retrieved from the Protein Data Bank (1D12) was used as the interaction model [37]. Energetically the most favorable conformation of the docked structure was selected on the basis of the LigandFit score and visual inspection. Initially hydrogen atoms were added to the protein, considering all the residues at their neutral form. The active site of 1D12 was defined from receptor cavity and was chosen to include not only the active site but also significant portions of surrounding surface. The grids were 842 points and the stereoview of the compounds with higher and lower in vivo anti-tumor activities intercalating toward  $d(\text{CGATCG})_2$  was described in Fig. 8a and b, respectively. Fig. 8 indicates that the 9-benzyl significantly influences the docking of **6a–p** into the cavity of  $d(\text{CGATCG})_2$ . Only when 9-benzyl is out of the cavity the planar  $\beta$ -carboline ring may be comfortably sandwiched between the base pairs of  $d(\text{CGATCG})_2$  and thus allows to form more hydrogen bonds between the amino acid residue and the base pairs of  $d(\text{CGATCG})_2$ . When 9-benzyl is in the cavity the planar  $\beta$ -carboline ring may be uncomfortably sandwiched between the base pairs of  $d(\text{CGATCG})_2$  and thus allows to form less or no hydrogen bonds between the amino acid residue and the base pairs of  $d(\text{CGATCG})_2$ .

To clarify the differences of the docking interactions of **6b,d,e,h,i,l,m,p** and **6a,c,f,g,j,k,n,o** with  $d(\text{CGATCG})_2$  the stereoview of the most potent compounds **6b,m** and the least potent compounds **6a,j** docking onto  $d(\text{CGATCG})_2$  was analyzed based on Fig. 9. From the stereoview it was found that a suitable docking consists of a comfortable insertion of  $\beta$ -carboline ring in the DNA base pairs and enough hydrogen bonds between the amino acid residue and the DNA base pairs. For instance, by comfortably inserting  $\beta$ -carboline ring into the base pairs of  $d(\text{CGATCG})_2$  eight hydrogen bonds were simultaneously formed between the L-Ala residue of **6b** and the base pairs of  $d(\text{CGATCG})_2$ . The same docking interactions were also found between **6m** and  $d(\text{CGATCG})_2$ . While docking **6a** onto  $d(\text{CGATCG})_2$  it results in an uncomfortable insertion of  $\beta$ -carboline ring in the DNA base pairs and forming no hydrogen bonds between the amino acid residue and the DNA base pairs. The same docking interactions were also found between **6j** and  $d(\text{CGATCG})_2$ .

## 3. Conclusion

In conclusion, novel *N*-(3-carboxyl-9-benzyl- $\beta$ -carboline-1-yl)ethylamino acids **6a–p** were prepared in acceptable yields using the seven-step route described above. In vitro cytotoxicity assays against five human carcinoma cell lines explored the cell selective

anti-proliferation for individual compounds. In vivo assays with S180 mice revealed eight active anti-tumor compounds, with four compounds being equipotent with the positive control cytarabine. Compounds **6a–p** neither decreased the immunologic function nor lowered the body weight increase of the treated S180 mice. By comparing the UV, CD and fluorescence spectra of CT DNA alone to those of a combination of CT DNA plus **6b**, an intercalating mechanism was identified. Docking **6a–p** onto  $d(\text{CGATCG})_2$  oligonucleotides explored that the 9-benzyl of **6a–p** to be out of the cavity of  $d(\text{CGATCG})_2$ , the planar  $\beta$ -carboline ring properly sandwiched between the base pairs of  $d(\text{CGATCG})_2$ , and enough hydrogen bonds occurred between **6a–p** and the base pairs of  $d(\text{CGATCG})_2$  were essential for in vivo anti-tumor activity.

## 4. Experimental

### 4.1. General

All chemicals were purchased from commercial suppliers and were purified when necessary. Protected amino acids with L-configuration were purchased from sigma chemical Co. Chromatography was performed on Qingdao silica gel H. The purities of the intermediates and the products were measured by TLC analysis (Merck silica gel plates of type 60 F<sub>254</sub>, 0.25 mm layer thickness) and HPLC analysis (waters, C<sub>18</sub> column, 4.6 × 150 mm). Melting points were determined in capillary tubes on an electrothermal SM/XMP apparatus without correction. UV spectra were measured on Shimadzu UV 2550. FT-IR spectra were run on an infrared spectrometer. ESI-MS was determined by Micromass Quattro micro TM API, Waters Co. <sup>1</sup>H NMR (500 Hz) and <sup>13</sup>C NMR (125 Hz) spectra were acquired on a Bruker AC 300 spectrometer in CDCl<sub>3</sub> or in DMSO-*d*<sub>6</sub> with TMS as internal standard, and chemical shifts are expressed in ppm ( $\delta$ ). Optical rotations were determined with a Jasco P-1020 Polarimeter. Statistical analysis of all the biological data was carried out by use of ANOVA test,  $p < 0.05$  is considered significant.

### 4.2. General procedure for preparing amino acid methyl esters

At 0 °C, 3.75 ml (50 mmol) of SOCl<sub>2</sub> was added dropwise to 50 ml of MeOH. After stirring at room temperature for 0.5 h, 42 mmol of L-amino acid was added, and then the reaction mixture was evaporated under vacuum. The residue was solidified and the title compounds were obtained as colorless powders in yields ranging from 85% to 99%.

### 4.3. Methyl 1-(2,2-dimethoxyethyl)-1,2,3,4-tetrahydro- $\beta$ -carboline-3-carboxylate (**1**)

A suspension of 5.0 g (24.510 mmol) of L-tryptophan methyl ester, 50 ml of MeOH and 6.0 ml (23.6 mmol) of 1,1,3,3-tetramethoxypropane

was adjusted to pH 1–2 with HCl (5 N) and stirred at 45 °C for 48 h. After cooling, the solvent was evaporated under vacuum, the residue was diluted with water and the aqueous solution was extracted with EtOAc (30 ml  $\times$  3). The organic phase was separated, washed successively with 10% sodium carbonate and saturated NaCl, dried over anhydrous sodium sulfate, filtered and the filtrate was evaporated under vacuum. The residue was purified by silica gel chromatography (CHCl<sub>3</sub>:MeOH, 30:1) to provide 1.57 g (29%) of (1S,3S)-**1** and 3.24 g (60%) of (1R,3S)-**1** as pale yellow oil. FAB-MS (*m/z*) 319 [M + H]<sup>+</sup>.

#### 4.4. Methyl 1-(2,2-dimethoxyethyl)- $\beta$ -carboline-3-carboxylate (**2**)

A mixture of 4.3 g (13.522 mmol) of **1** and 100 ml of DMF was stirred at 0 °C until a clear solution was formed, to which 3.04 g (19.296 mmol) of KMnO<sub>4</sub> was then added. The reaction mixture was stirred at 0 °C for 1 h, and then at room temperature for 3 h until TLC (CHCl<sub>3</sub>:MeOH, 15:1) indicated the complete disappearance of starting material. The formed precipitate was filtered and the filtrate was evaporated under vacuum. The residue was diluted with 100 ml of EtOAc, and the solution was washed successively with water and saturated aqueous NaCl. The organic phase was separated and dried over anhydrous sodium sulfate. After filtration, the filtrate was evaporated under vacuum. The residue was solidified in acetone to give 3.47 g (80.3%) of the title compound as a yellow power.

#### 4.5. Methyl 9-benzyl-1-(2,2-dimethoxyethyl)- $\beta$ -carboline-3-carboxylate (**3**)

A mixture of 5.50 g (17.525 mmol) of **2**, 20 ml of anhydrous DMF and 20 ml of anhydrous THF was stirred to form a clear solution, and then 1.05 g (26.32 mmol, 60%) of NaH was added. The mixture was stirred at room temperature for 30 min, benzyl bromide (2.98 g, 17.427 mmol) was added and the reaction mixture was stirred for 4 h. To this mixture, 200 g of ice was added and the solution was extracted with EtOAc (100 ml  $\times$  3). The organic phase was separated, washed with saturated aqueous NaCl, and dried over anhydrous sodium sulfate. After filtration the filtrate was evaporated under vacuum. The residue was purified with silica gel chromatography (petroleum ether:acetone, 2:1) to give 4.337 g (61.2%) of the title compound as colorless powder.

#### 4.6. 2-(3-Methoxycarbonyl-9-benzyl- $\beta$ -carboline-1-yl) acetaldehyde (**4**)

A mixture of 1.0 g (2.475 mmol) of **3**, 14 ml of HOAc and 2 ml of water was stirred at room temperature for 16 h. To the reaction mixture 200 g of ice was added. The formed precipitates were collected by filtration to provide 538 mg (60.7%) of the title compound which was used directly in the next reaction without purification.

#### 4.7. General procedure for preparing N-(9-benzyl-3-carboxyl- $\beta$ -carboline-1-yl)-ethylamino acid methyl esters (**5a–o**)

A mixture of 2.0 mmol of amino acid methyl ester, 1.33 mmol of NaOH, 25 ml of MeOH and 476 mg (1.33 mmol) of **4** was stirred at room temperature for 10 min, and then 58.2 mg (0.931 mmol) of NaBH<sub>3</sub>CN was added. The reaction mixture was stirred at room temperature for 4 h, adjusted to pH 1–2 with HCl (3 N) and evaporated under vacuum. The residue was diluted with 20 ml of water, and the aqueous solution was washed with ether (30 ml  $\times$  3). The aqueous phase was adjusted to pH 8 with aqueous NaOH (1 N), extracted with EtOAc (100 ml  $\times$  3), and the organic phase was separated and washed with saturated aqueous NaCl, and dried over anhydrous sodium sulfate. After filtration the solvent was

evaporated under vacuum, and the residue was purified by silica gel chromatography to give **5a–p** in 35.0–88.0% yields.

#### 4.8. General procedure for preparing N-(9-benzyl-3-carboxyl- $\beta$ -carboline-1-yl)-ethylamino acid (**6a–p**)

At 0 °C, 2 ml methanolic NaOH solution (2 N) was added to a solution of **5a–p** (1.12 mmol) in 8 ml of MeOH and 8 ml of CHCl<sub>3</sub>. The reaction mixture was stirred at 0 °C for 10 h. TLC analysis (CHCl<sub>3</sub>:MeOH:HOAc, 5:1:0.2) indicated complete disappearance of **5a–p**. The resulting mixture was adjusted with HCl (2 N) to pH 2 and the solvent was evaporated under vacuum. The residue was dissolved in 50 ml of EtOAc and the solution was washed successively with 5% sodium bicarbonate, 5% citric acid, and saturated NaCl and then dried over anhydrous sodium sulfate. After filtration and evaporation under reduced pressure, products **6a–p** were obtained in 52–72% yields.

#### 4.9. In vitro cytotoxic assay

Cytotoxic assays in vitro were carried out using 96-well plate cultures and MTT staining according to the procedure described by Al-Allaf et al. with slight modification. The human-derived cell lines H1299 (human non-small cell lung carcinoma), HepG<sub>2</sub> (human liver carcinoma), Hela (human cervical carcinoma), HL-60 (human immature granulocyte leukemia) and MES-SA (human sarcoma cell) lines were cultured in DMEM or RPMI-1640 (Gibco) medium containing 10% (v/v) fetal bovine serum and 10,000 U/ml penicillin and 100  $\mu$ g/ml streptomycin. Cell suspension (100  $\mu$ l of  $5 \times 10^4$  cells/ml) was seeded in 96-well plates and incubated at 37 °C in a humidified atmosphere of 5% CO<sub>2</sub> for 4 h. The medium was replaced by medium containing different concentrations (ranging from 0.1  $\mu$ M to 400  $\mu$ M) of **6a–p**, which were dissolved in DMSO vehicle. The vehicle control received only DMSO (1%, v/v). To the wells, 25  $\mu$ l of medium containing test samples of different concentrations of **6a–p** was added. After 48 h, 25  $\mu$ l (final concentration, 0.5 mg/ml) of MTT (Sigma) was added to each well, and the solutions incubated for an additional 4 h. Then culture medium was removed. The resulting MTT-formazan product was dissolved in 100  $\mu$ l DMSO. The amount of formazan was determined by measuring the optical density at 570 nm. The cytotoxic activities were observed to occur in a dose-dependent manner in the cells. The activity was expressed as an IC<sub>50</sub> value, which is the concentration of test sample to give 50% inhibition of the growth of tumor cells.

#### 4.10. In vivo anti-tumor assay

Male ICR mice, purchased from Peking University Health Science Center, were maintained at 21 °C with a natural day/night cycle in a conventional animal colony. The mice were ten to twelve weeks old at the beginning of the experiments. S180 ascites tumor cells were used to form solid tumors after subcutaneous injection. For initiation of subcutaneous tumors the cells were obtained as an ascitic form from the tumor-bearing mice, which were serially transplanted once per week. Subcutaneous tumors were implanted by injecting 0.2 ml of 0.9% saline containing  $1 \times 10^7$  viable tumor cells under the skin on the right armpit. Twenty-four hours after implantation, the mice (twelve per group) were randomly divided into experimental groups. The mice of the positive control group were given a daily i.p injection of 89  $\mu$ mol/kg of cytarabine in 0.2 ml of 0.9% saline for seven consecutive days. The mice of the negative control group were given a daily i.p injection of 0.2 ml of 0.9% saline for seven consecutive days. The mice of the treatment groups were given a daily i.p injection of 89  $\mu$ mol/kg of **6a–p** in 0.2 ml of 0.9%

saline for seven consecutive days. The weights of animals were recorded everyday. Twenty-four hours after the last administration, all mice were weighed, sacrificed by diethyl ether anesthesia and dissected to immediately obtain and weigh the tumor and spleen samples. The inhibition ratio was calculated based on inhibition ratio (%) =  $[(A - B)/A] \times 100$ , wherein *A* is average tumor weight of the negative control, and *B* is that of the treatment group.

#### 4.11. Acute toxicities assay

ICR mice were maintained at 21 °C with a natural day/night cycle in a conventional animal colony. The mice were ten to twelve weeks old at the beginning of the experiments. The sterile food and water were provided according to the institutional guidelines. Prior to each experiment, mice were fastened overnight and allowed free access to water. The mice were given an i.p. injection of 150, 300 or 500 mg/kg **6a-p** in 0.2 ml of 0.9% saline. Each group contained 12 mice (six males and six females). After the injection the mice were monitored continuously for up to 7 days to observe any abnormal behavior or death. All mice were sacrificed on the 7th day and checked macroscopically for possible damage to the heart, liver, and kidneys. LD<sub>50</sub> values were calculated graphically.

#### Acknowledgments

This work was finished in Beijing Area Major Laboratory of Peptide and Small Molecular Drugs, supported by PHR (IHLB, KZ200810025010), the National Natural Science Foundation of China (30672513) and Special Project (2008ZX09401-002) of China.

#### Appendix. Supplementary data

The chemical and physical data of compounds **2**, **3**, **5a-p** and **6a-p**: These materials are available free of charge via the Internet at <http://www.sciencedirect.com/>.

Supplementary data associated with this article can be found in the online version, at doi:10.1016/j.ejmech.2009.05.006.

#### References

- [1] G. Momekov, A. Bakalova, M. Karaivanova, *Curr. Med. Chem.* 12 (2005) 2177–2191.
- [2] L.H. Hurley, *Nat. Rev. Cancer* 2 (2002) 188–200.
- [3] R. Martinez, L. Chacon-Garcia, *Curr. Med. Chem.* 12 (2005) 127–151.
- [4] W.D. Wilson, R. Jones, in: M.S. Whittingham, A.J. Jacobson (Eds.), *Intercalation Chemistry*, Academic, New York, 1981 (Chapter 14).
- [5] W.O. Foye (Ed.), *Cancer Chemotherapeutic Agents*, American Chemical Society, Washington, DC, 1995.
- [6] C.L. Propst, T.L. Perun (Eds.), *Nucleic Acid Targeted Drug Design*, Marcel Dekker, New York, 1992.
- [7] S. Antony, K.K. Agama, Z.H. Miao, *Mol. Pharmacol.* 70 (2006) 1109–1120.
- [8] L.V. Flores, A.M. Staples, H. Mackay, *Chembiochem* 7 (2006) 1722–1729.
- [9] L.J. Xie, X.H. Qian, J.N. Cui, *Bioorg. Med. Chem.* 16 (2008) 8713–8718.
- [10] P. Wanda, F. Pognan, L. Kaczmarek, J. Boratynski, *J. Med. Chem.* 37 (1994) 3503–3510.
- [11] C.A. Gandolfi, G. Beggiolin, E. Menta, M. Palumbo, C. Sissi, S. Spinelli, F. Johnson, *J. Med. Chem.* 38 (1995) 526–536.
- [12] A. Bolognese, G. Correale, M. Manfra, *J. Med. Chem.* 47 (2004) 849–858.
- [13] M.A. Lynch, O. Duval, A. Sukhanova, J. Devy, S.P. Mackay, R.D. Waigh, I. Nabiev, *Bioorg. Med. Chem. Lett.* 11 (2001) 2643–2646.
- [14] T. Nakanishi, M. Suzuki, A. Mashiba, K. Ishikawa, T. Yokotsuka, *J. Org. Chem.* 63 (1998) 4235–4239.
- [15] J. Jimenez, L. Riveron-Negrete, F. Abdullaev, *Exp. Toxicol. Pathol.* 60 (2008) 381–389.
- [16] H.J. Guan, H.S. Chen, W.L. Peng, *Eur. J. Med. Chem.* 41 (2006) 1167–1179.
- [17] J. Ishida, H.K. Wang, K.F. Bastow, C.Q. Hu, K.H. Lee, *Bioorg. Med. Chem. Lett.* 9 (1999) 3319–3324.
- [18] T.A.K. Al-Allaf, L.J. Rashan, *Eur. J. Med. Chem.* 33 (1998) 817–820.
- [19] R. Cao, W. Peng, H. Chen, Y. Ma, X. Liu, X. Hou, H. Guan, A. Xu, *Biochem. Biophys. Res. Commun.* 338 (2005) 1557–1563.
- [20] F. Pognan, J.M. Saucier, C. Paoletti, L. Kaczmarek, P. Nantka-Namirski, M. Mordarski, W. Peczyńska-Czoch, *Biochem. Pharmacol.* 44 (1992) 2149–2155.
- [21] M. Laronze, M. Boisbrun, S. Leonce, B. Pfeiffer, P. Renard, O. Lozach, L. Meijer, A. Lansiaux, C. Bailly, J. Sapi, J.Y. Laronze, *Bioorg. Med. Chem.* 13 (2005) 2263–2283.
- [22] Y. Funayama, K. Nishio, K. Wakabayashi, M. Nagao, K. Shimoi, T. Ohira, S. Hasegawa, N. Saijo, *Mutat. Res.* 349 (1996) 183–191.
- [23] A.M. Sobhani, S.A. Ebrahimi, M.J. Mahmoudian, *J. Pharm. Pharm. Sci.* 5 (2002) 19–23.
- [24] M. Zhao, L. Bi, W. Wang, C. Wang, M. Baudy-Floc, J. Ju, S. Peng, *Bioorg. Med. Chem.* 14 (2006) 6998–7010.
- [25] H. Gonzalez-Diaz, F. Prado-Prado, F.M. Ubeira, *Curr. Top. Med. Chem.* 8 (2008) 1676–1690.
- [26] H. Gonzalez-Diaz, S. Vilar, L. Santana, E. Uriarte, *Curr. Top. Med. Chem.* 7 (2007) 1015–1029.
- [27] M.C. Rosales-Hernandez, J. Bermúdez-Lugo, J. Garcia, J. Trujillo-Ferrara, J. Correa-Basurto, *Anticancer Agents Med. Chem.* 9 (2009) 230–238.
- [28] R. Dias, W.F. de Azevedo Jr., *Curr. Drug Targets* 9 (2008) 1040–1047.
- [29] N. Li, Y. Ma, C. Yang, L.P. Guo, X.R. Yang, *Biophys. Chem.* 116 (2005) 199–205.
- [30] D. Suman, S.K. Gopinatha, *J. Mol. Struct.* 872 (2008) 56–63.
- [31] U. Varadarajan, C. Alfonso, U.N. Balachandran, *Polyhedron* 26 (2007) 3008–3016.
- [32] P.U. Aheswari, M. Alaniandavar, *J. Inorg. Biochem.* 98 (2004) 219–230.
- [33] R.P. Queiroz, M.S. Elisabete Castanheir, C.T. Teresa Lopes, K. Yvonne Cruz, *J. Photochem. Photobiol., A* 190 (2007) 45–52.
- [34] A.R. Shaikh, M. Ismael, C.A.D. Carpio, H. Tsuboi, M. Koyama, A. Endou, M. Kubo, E. Broclawik, A. Miyamoto, *Bioorg. Med. Chem. Lett.* 16 (2006) 5917–5925.
- [35] M.R. Doddareddy, Y.S. Cho, H.Y. Koh, A.N. Pae, *Bioorg. Med. Chem.* 12 (2004) 3977–3985.
- [36] A.M. Sobhani, S.R. Amini, J.D.A. Tyndall, E. Azizi, M. Daneshlatab, A. Khalaj, *J. Mol. Graph. Model.* 25 (2006) 459–469.
- [37] C.M. Venkatachalam, X. Jiang, T. Oldfield, M. Waldman, *J. Mol. Graph. Model.* 21 (2003) 289–307.